ISSN 2079-1704. Хімія, фізика та технологія поверхні. 2021. Т. 12. № 3. С. 157-167

PACS: 31.15.A-; 31.15.ap; 31.15.bu; 31.15.E-; 31.70.Dk; 36.40.-c doi: 10.15407/hftp12.03.157

V.M. Gun'ko

QUANTUM-CHEMICALLY COMPUTED INTEGRAL CHARACTERISTICS OF COMPLEX NANOMATERIALS

Chuiko Institute of Surface Chemistry of National Academy of Sciences of Ukraine
17 General Naumov Str., Kyiv, 03164, Ukraine, E-mail: vlad_gunko@ukr.net

Development of theoretical tools to analyze electronic structure of complex nanomaterials depending on features of spatial and chemical organizations of different phases is of interest from both practical and theoretical points of view. Therefore, in this work, an approach based on computations of the atomic charge distribution functions (CDF) in parallel to calculations of the distribution functions of the chemical shifts (SDF) of protons is developed to be applied to a set of complex oxide and carbon nanomaterials. Binary nanooxides (alumina/silica, titania/silica), 3d-metal-doped anatase, activated carbon, carbon nanotube, fullerene C_{60}, graphene oxide, and N-doped Kagome graphene are considered here as representatives of different classes of nanomaterials. The analyses of the CDF and SDF as nonlocal characteristics of certain kinds of atoms in complex systems provide a deeper insight into electronic structure features depending on composition of the materials, guest phase-doped host phase at various amounts of dopants, structure of O- and OH-containing surface sites, amounts and organization of adsorbed water, formation of neutral and charged surface functionalities, bonding of solvated ions, etc. The CDF of metal and hydrogen atoms (electron-donors) are more sensitive to the mentioned factors than the CDF of O, N, and C atoms (electron acceptors) in various systems. As a whole, the use of the CDF and SDF in parallel expands the tool possibility in detailed analysis of the structural and interfacial effects in dried and wetted complex nanomaterials.

***Keywords**: complex nanomaterials, atomic charges, chemical shifts of protons, distribution functions, DFT method, semiempirical method*

INTRODUCTION

Composition and phase or dopant distributions in particles of complex nanomaterials may strongly affect the properties and characteristics of whole systems [1–12]. First, new active surface sites (*e.g.*, bridging $\equiv M_1OM_2\equiv$, $\equiv M_1O(H)M_2\equiv$ at M_1 = Si and M_2 = Al, Ti, *etc*.), absent in individual components, appear in the complex systems. These sites are important for adsorption, catalytic acid-base reactions, interactions with filled polymers, drugs in drug delivery systems, *etc*. [5–9]. Second, doping of a main phase (*e.g.*, C, TiO_2, ZnO, *etc*.) by various dopants (*e.g.*, 3d metals, N, P, S, *etc*.) changes the upper valence band and band gap that is of importance for catalytic redox reactions, electron conductivity, *etc*. [13]. Third, the mechanical and thermal properties of the materials depend on composition and phase distributions in composites [15–17]. Practically all the characteristics and properties of complex nanomaterials could be varied due to changes in their structure, composition, and phase distributions at a nano-scale level [1–17]. Therefore, accurate modeling of the nanostructures, appropriate description and evaluation of the interphase interactions in complex nanomaterials are of importance for correct analyses of their practically important characteristics and properties.

There are several aspects related to the models and methods used in quantum chemical modeling of complex materials [18–22]. First, it is of importance to select methods (*ab initio*, density functional theory (DFT), semiempirical, *etc*.) appropriate to solve the tasks. Second, the use of adequate basis sets (narrow or extended, optimal, maximum appropriate), correct account of electron correlation and exchange (perturbation theory in *ab initio*, various functionals in DFT, additional tools), as well as corrections on the basis set superposition errors (BSSE), temperature, zero-point energy, and vibrations are quite important. Third, accurate selection of appropriate models (clusters, nanoparticles, primitive or expanded cells used with periodic boundary conditions (PBC), *etc*.) is necessary. Additionally, taking into account solvation, kinetic and dynamic aspects and some others could be important on the analyses of the phenomena occurring at a surface of complex nanostructured systems under various conditions [18–22]. Therefore, in the present work, several

aspects related mainly to the sizes of particulate models, their phase compositions, structure of the host and gest phases, bound water effects, as well as the types of the materials (*e.g.*, metal and metalloid oxides, various carbons) are analyzed. It has been done using *ab initio* (6-31G(d,p) and DGDZVP basis sets), DFT (functional ωB97X–D with the cc–pVDZ basis set) [23–25]. Some calculations have been performed using a solvation model with the SMD method [26] and gauge-including-atomic-orbital (GIAO) method [27, 28] to compute ^{1}H NMR spectra. Semiempirical PM7 and PM6 methods [29, 30] have been applied to large models.

CALCULATION METHODS

Individual materials (oxide and carbon nanoparticles) and complex models hydrated by water clusters or interfacial water layer located at a solid surface are analyzed using the Gaussian 09 [27], GAMESS 2020 R2 [28], and MOPAC 2016 [29, 30] program suits. The DFT calculations have been done using a hybrid functional ωB97X–D with the cc–pVDZ basis set. The GIAO method (with DFT) has been used to compute the chemical shifts of the proton resonance (δ_H) [27, 28]. The solvation effects have been analyzed with the SMD method [26–28] implemented in the Gaussian and GAMESS program suits. The calculations have been carried out taking into account zero-point and thermal corrections to the Gibbs free energy in the gas phase and for solvated molecules and solids clusters using the geometry optimized with ωB97X–D/cc–pVDZ (with or without SMD). Note that ωB97X–D introduces empirical damped atom-pairwise dispersion terms into the functional containing range-separated Hartree-Fock (HF) exchange for better description of van-der-Waals interactions [24, 25]. Therefore, ωB97X–D has been selected to obtain more adequate results for the gas and liquid phases interacting with nanoparticles. The distribution functions of various parameters have been calculated with a simple equation [31–34]

$$f_n(X) = (2\pi\sigma_n^2)^{-0.5} \sum_j \frac{\exp[-(X_{n,j} - X)^2]}{2\sigma_n^2}, \qquad (1)$$

where j is the number of a certain type (n) of atoms, $\sigma^2$is the distribution dispersion, and X_j is the value of atomic charge (CDF) (Figs. 1–7) or chemical shift δ_H (SDF) (Figs. 8 and 9), and X is the current value. For the electron-donor atoms (H, Si) σ = 0.01–0.025 a.u. is used, and σ = 0.05 a.u. for electron-acceptor (O, C, N) atoms [34]. To decrease small details (*e.g.*, small excess peaks) in the distribution functions, the distribution dispersion could be increased, *e.g.*, up to the values corresponding to experimental peaks (*i.e.*, full width at the half-height, FWHH) [10, 35]. The distribution functions of various characteristics (*e.g.*, *q, δ, etc*.) based on the data of any quantum chemical method may be calculated using Eq.(1). Several silica, alumina, titania, and complex oxide clusters have been studied with initial structures with (i) 22 units with silica/16OH or anatase/10OH, (ii) 44 units with silica/24OH, and (iii) 88 units with silica/40OH without or with sorbed water with a solvation model SMD. These and some other clusters are doped by various dopants (oxides of Si, Ti, Al, Fe, Ni, Zn, and Sn) and computed with *ab initio* (restricted HF (RHF) method with the 6–31G(d,p) and DGDZVP basis sets) or DFT methods. The alumina cluster with 111 units is used as a model of γ–Al_2O_3. Carbon nanomaterials (activated carbon (AC), carbon nanotube (CNT), graphene oxide (GO), fullerene C_{60} (fullerite), and nitrogen-doped Kagome graphene (NKG)) are modelled using the PM7 and PM6 methods. Note that NKG was recently described in detail [36].

RESULTS AND DISCUSSION

Practically in all the models of complex nanooxides calculated using the *ab initio* and DFT methods with different basis sets, the CDF demonstrate significant changes in peak positions and band width due to doping of the main (host) phase (SiO_2 or TiO_2) by various metal (Al, Ti (Figs. 1 and 2), Al (Fig. 2), Zn (Fig. 3), Ni (Fig. 4), Sn (Fig. 5), and Fe (Fig. 6)) oxides. For complex carbon nanomaterials (AC, CNT, GO, fullerite, and NKG) (Fig. 7), the CDF strongly differ in the shape and peak positions in comparison to nanooxides due to lower polarity of the skeletal bonds in carbon materials, which are, therefore, mainly hydrophobic (especially, non-functionalized carbons). Therefore, for all the carbons modelled, the q_C CDF are located around $q_C = 0$. However, for all atoms in oxides, the CDF are located far from $q = 0$ at $q > 0$ (metals, H) or $q < 0$ (oxygen).

In the anatase clusters (22 units with ten surface hydroxyls) doped by silica, the bond polarity decreases with increasing number of the Si atoms.

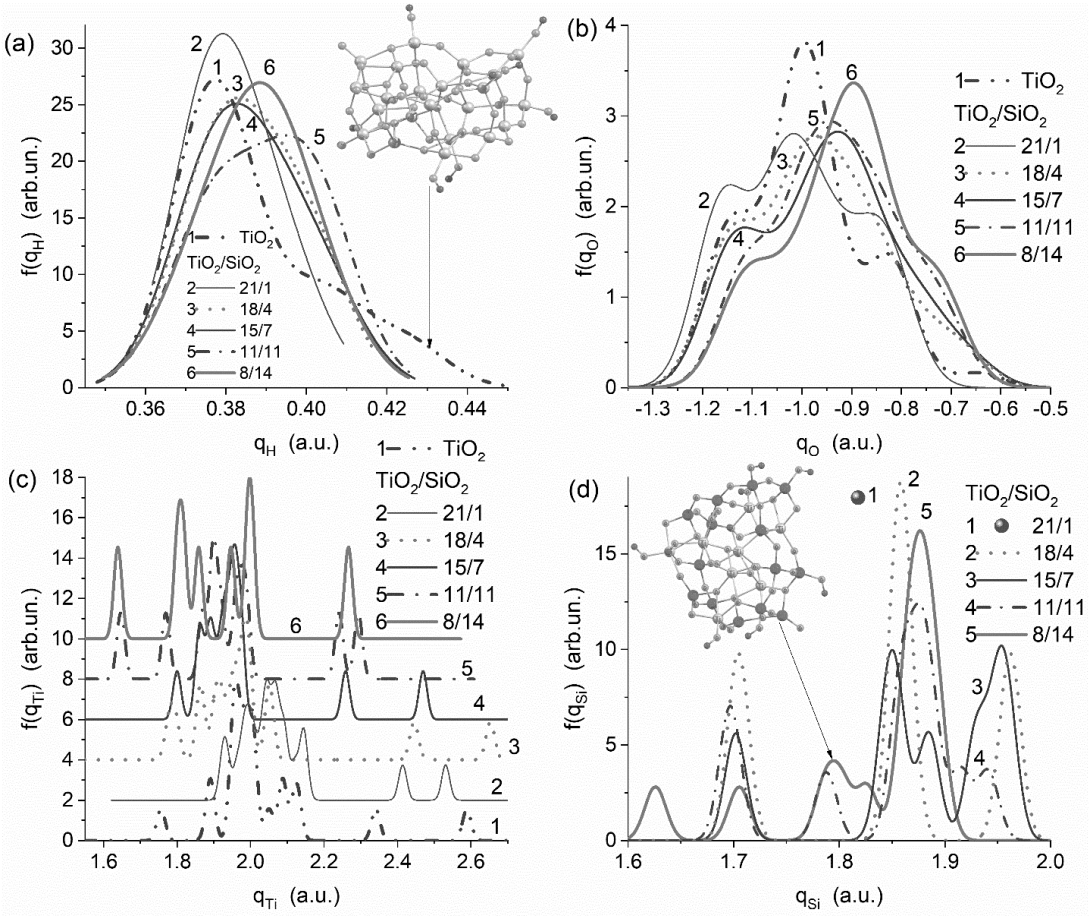

Fig. 1. Effects of the Ti/Si ratio in the TiO_2/SiO_2 clusters with 22 polyhedra (with 10OH) of the initial anatase structure doped silicon dioxide on the atomic charge distribution functions for: (*a*) H, (*b*) O, (*c*) Ti, and (*d*) Si atoms (restricted HF (RHF) calculations with the 6-31G(d,p) basis set)

There is a tendency of a decrease in the atomic charges of Ti (Fig. 1 *c*) and Si (Fig. 1 *d*), as well as in excess electron density located on the O atoms (Fig. 1 *b*), with decreasing Ti/Si ratio. For the H atoms, there is the opposite tendency with increasing charges upon decreasing Ti/Si (Fig. 1 *a*). This is typical for the Brønsted acidity of complex oxides *vs*. their composition. Note that the q_H CDF shape changes with doping. The H atoms with maximal charges of 0.42–0.44 a.u. are absent in the doped clusters, but the main peak of q_{Ti} CDF for the former is located at minimal q_{Ti} values (Fig. 1 *a*, curve 1). This is in agreement with increasing Brønsted acidity of the bridging hydroxyls ≡SiO(H)Ti≡ in comparison to the hydroxyls in the individual silica and titania phases. Note that the Brønsted acidity of ≡SiO(H)Al≡ is greater than that of ≡SiO(H)Ti≡ (Fig. 2 *a*) due to a lower number of valence electrons in Al than in Ti. Not only the Ti/Si or Al/Si ratio affects the surface hydroxyl acidity but also solvation evaluated using the supercluster approach or SMD method. It enhances the O–H bond polarity and possibility of the appearance of mobile protons forming Eigen (H_3O^+) ($q_H \approx 0.32$ a.u. in Fig. 2 *a*) or Zundel ($H_5O_2^+$) cations. Enhancement of this effect due to the surroundings for the Si, Al, and Ti atoms in larger clusters (as well as due to solvation) causes broadening of the CDF peaks (Fig. 2 *c*, *d*). All these changes affect the properties of complex nanooxides in heterogeneous acid-base reactions, in which Brønsted and Lewis acid and base sites can play the main role. Not only particle compositions (*e.g.*, Al/Si or Ti/Si ratio) but also particle sizes and shapes can affect the

characteristics of active surface sites taking part in the adsorption of reagents with subsequent catalysis of various chemical transformation.

Anatase as a photocatalyst is active in redox reactions. However, its bandgap (E_g) is relatively large ($E_g \approx 3.2$ eV corresponding to ultraviolet light). Therefore, it cannot be used upon activation by visible light. To improve titania as a photocatalyst, it is doped by various dopants (metals and nonmetals) to provide $E_g < 2–3$ eV.

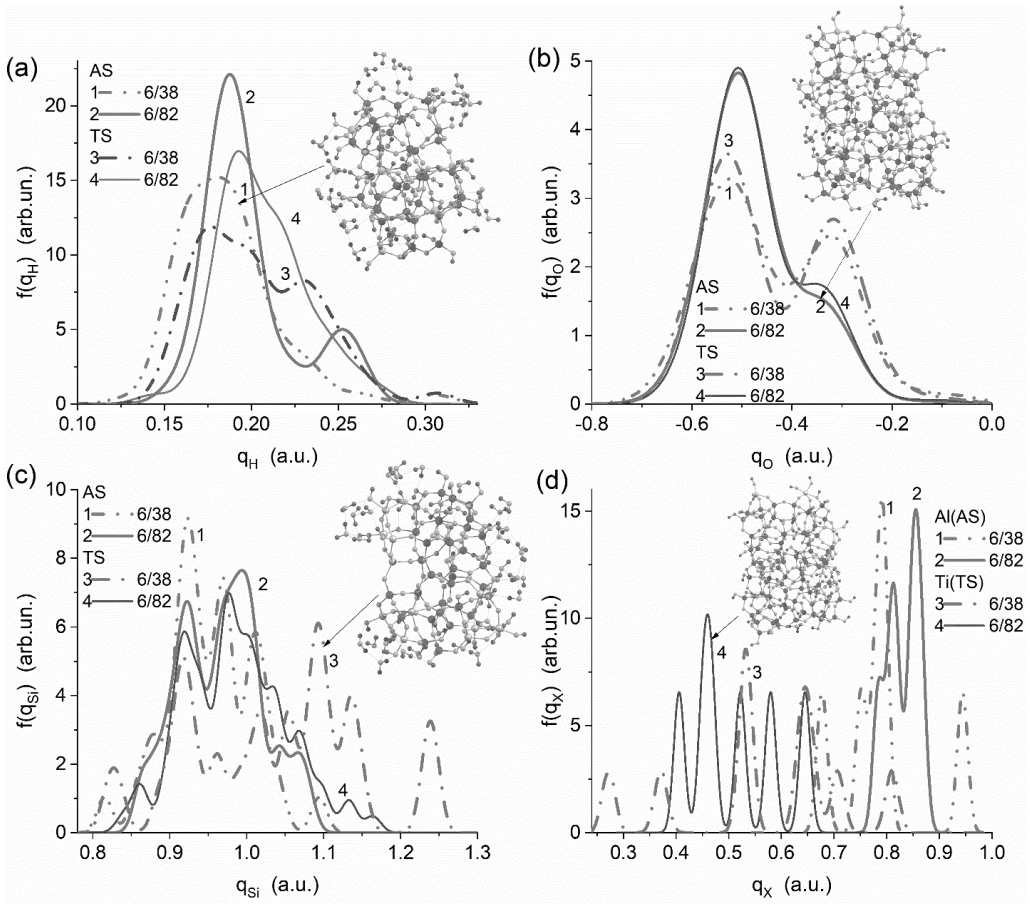

Fig. 2. Atomic charge distribution functions in the clusters of Al_2O_3/SiO_2 and TiO_2/SiO_2 with 44 units (with 30OH and 24OH, respectively, and bound $42H_2O$) and 88 units (46OH and 40OH, respectively, and bound $10H_2O$) with six units of Al_2O_3 or TiO_2 for (*a*) H, (*b*) O, (*c*) Si, and (*d*) Al and Ti atoms (DFT method with ωB97X–D/cc–pVDZ)

The effects of dopants of several types on the CDF are analyzed here (Figs. 3–6). Note that the effects on the bandgap were previously studied using quantum chemical methods and various approaches (*e.g.*, cluster or PBC), but the CDF were not yet computed for similar complex systems [34, 37]. Besides the appearance of excess electrons or holes, additional polarization of the oxygen-metal bonds can affect the band gap. The appearance of excess electron density caused by weakly bound electrons (number of valence electron in dopant metal atoms $n_X > 4 = n_{Ti}$) characterized by energy levels located higher than the top of the upper valence band of a pure host phase, as well as the holes ($n_X < 4$, located lower the conductive band bottom). In the electron-hole subsystem for the host/guest phases or for dopants embedded into the host phase and characterized by larger or smaller numbers of valence electrons than metal in a host phase (*e.g.*, Ti), their behavior may reflect in changes in the CDF (Figs. 3–6). The computing results show that the atomic charge distribution functions depend on the ratio of the guest/host phases and a kind of metal atoms (*i.e.*, metal oxide) embedded into a host phase. Typically, the positive effects (*i.e.*, diminution of the E_g value) are observed for a small guest/host

ratio (not greater than several atomic percent without formation of individual guest phase) [38–44]. Note that the CDF of metals in doped titania are more sensitive (and more important) to the mentioned ratio than that of other atoms (H and O).

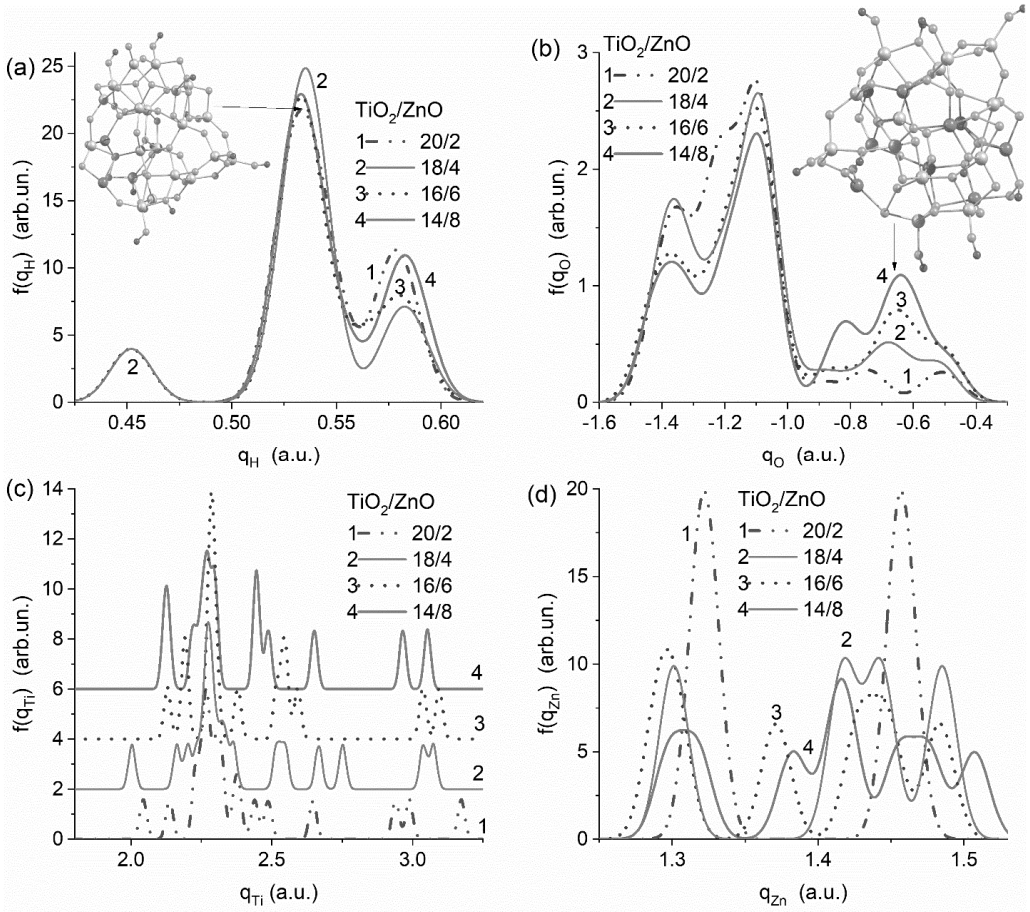

Fig. 3. Effects of the Ti/Zn ratio in the TiO_2/ZnO clusters with 22 polyhedra (with 10OH) on the atomic charge distribution functions for: (*a*) H, (*b*) O, (*c*) Ti, and (*d*) Zn atoms (RHF with the DGDZVP basis set)

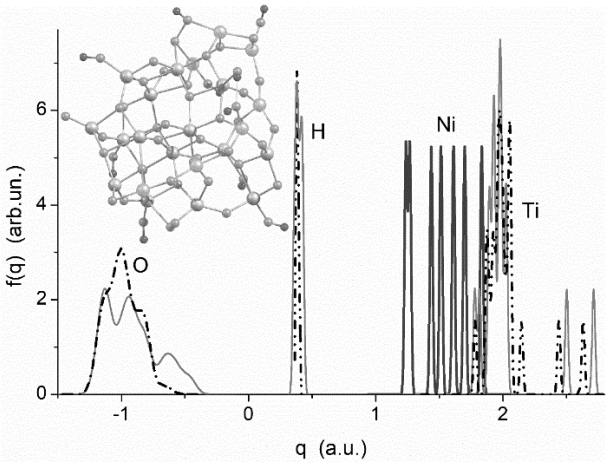

Fig. 4. Effects of the Ni atoms in the TiO_2/NiO cluster (Ni/Ti = 7/15) with 22 polyhedra (with 10OH) on the atomic charge distribution functions for H, O, Ti, and Ni atoms (solid lines) and the TiO_2 cluster (dot-dashed lines) (RHF with the 6-31G(d,p) basis set)

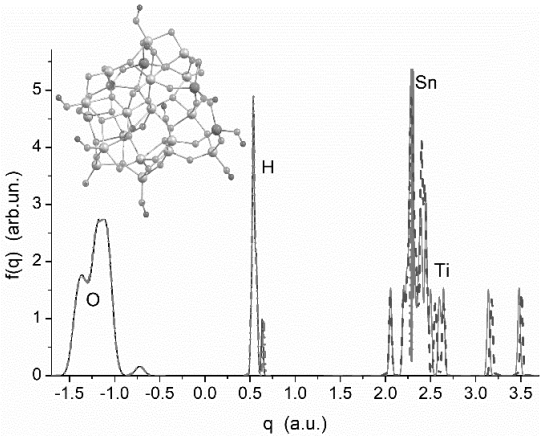

Fig. 5. Effects of the Sn/Ti ratio in the SnO_2/TiO_2 clusters (Sn/Ti = 2/20 (dot-dashed lines) and 3/19 (solid lines) with 22 polyhedra (with 10OH) on the atomic charge distribution functions for H, O, Ti, and Sn atoms (RHF with the DGDZVP basis set))

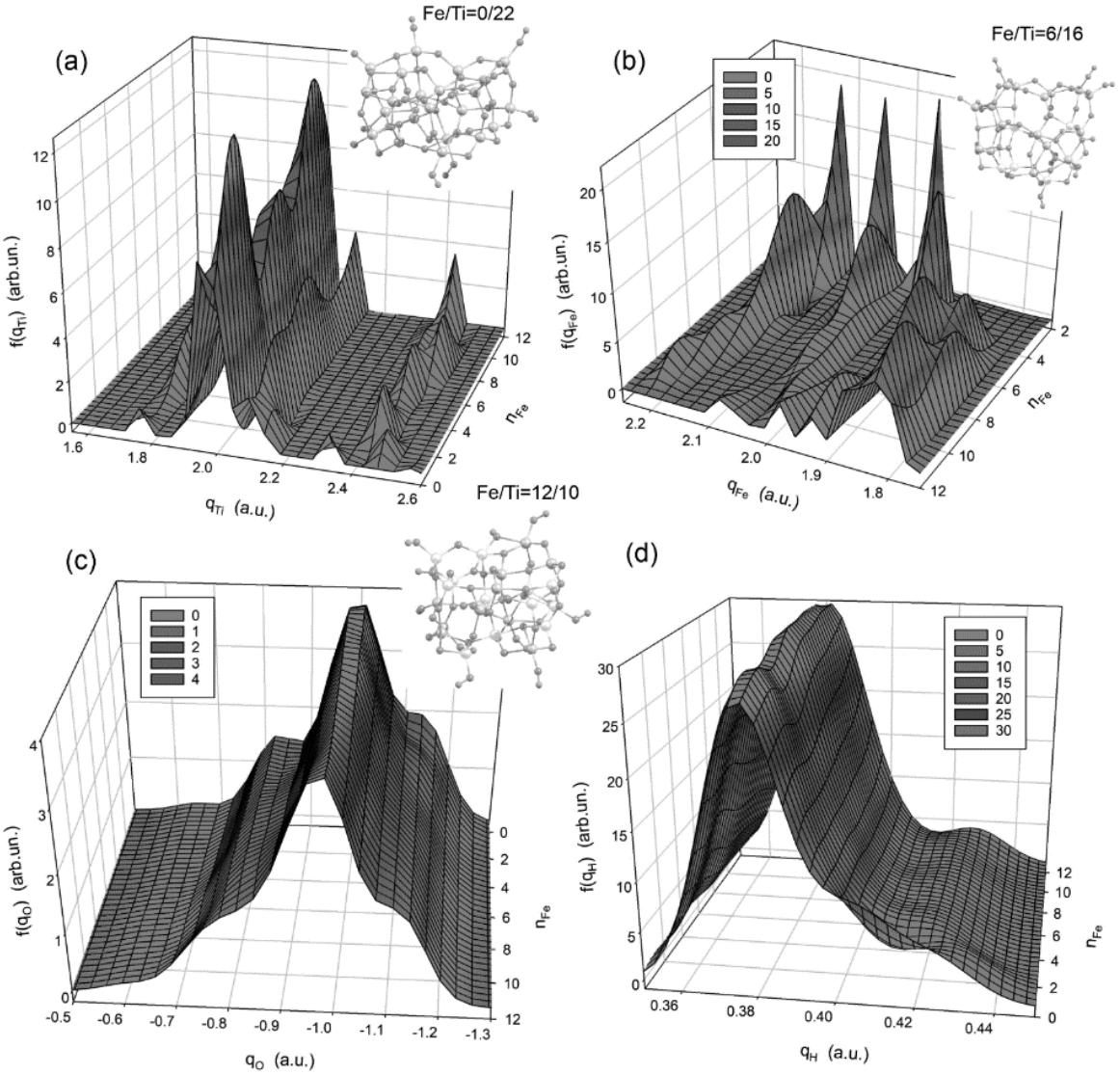

Fig. 6. Effects of the Fe atoms (n_{Fe} = 1, 2, 4, 6, 8, 10, and 12) in the Fe_2O_3/TiO_2 clusters with 22 polyhedra on the atomic charge distribution functions for: (*a*) Ti, (*b*) Fe, (*c*) O, and (*d*) H atoms (RHF with the 6-31G(d,p) basis set)

This is well visible on the 3D CDF surfaces for Fe-doped anatase (Fig. 6), since for the H and O atoms these functions are characterized by relatively smooth surfaces (Fig. 6 *c*, *d*) in contrast to that for the Fe and Ti atoms (Fig. 6 *a*, *b*). At small changes in the X/Ti ratio (*e.g.*, 2/20 and 3/19 for Sn/Ti, Fig. 5), the changes in the CDF for Sn and Ti are better visible than that for H and O. At relatively large X/Ti values (Figs. 3, 4, and 6), this tendency remains; however, changes in the H and O CDF become well visible, but the position of their main CDF peaks does not practically change.

The structural effects in carbon nanomaterials on the atomic charge distribution functions of the C, H, O, and N atoms are well visible (Fig. 7) for activated carbon (Fig. 7 *a*), capped carbon nanotube (Fig. 7 *b*), graphene oxide (GO) with two layers with bound water (Fig. 7 *c*) or single layer GO, wetted fullerite with fullerene C_{60} (Fig. 7 *a*, *e*) and nitrogen-doped Kagome graphene (NKG) (Fig. 7 *d*). Note that NKG with an open-work structure [36] remains plane upon the geometry optimization with the PM7 method (Fig. 7 *d*, insert). The behavior of the C CDF for pure or modified or functionalized carbon materials is characterized by a location of the main peak around $q_C = 0$ (Fig. 7). Oxidizing or doping (*e.g.*, by N or O) of carbons may lead to broadening or even splitting of the C CDF [45].

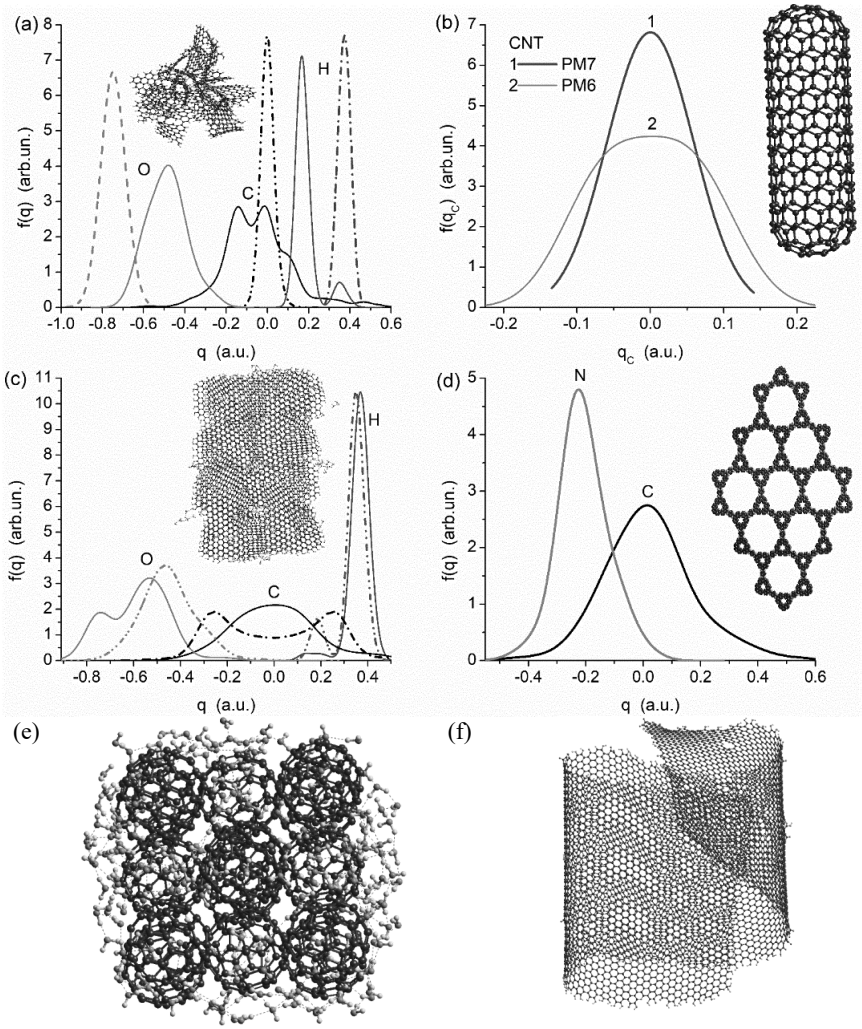

Fig. 7. Effects of the carbon nanomaterials structure on the atomic charge distribution functions for C, H, O, and N atoms for: (*a*) activated carbon (1589 atoms) with O-containing functionalities (solid lines) (insert) and vdW cluster with $14C_{60}$ solvated in a water shell ($213H_2O$) (dashed lines, structure is shown in (*e*)), (*b*) capped carbon nanotube with 260 atoms (PM6 and PM7 methods), (*c*) graphene oxide with two layers with bound water ($183H_2O$) (solid lines, 4438 atoms) (insert) and folded single-layer GO (dashed lines, 6358 atoms) (shown in (*f*)), and (*d*) nitrogen-doped Kagome graphene with 1488 C and 152 N atoms (PM7 method)

This corresponds to a decrease in the hydrophobicity of modified and functionalized carbons. There is an effect of 5-member rings in C_{60} and CNT resulting in broadening of the C CDF in comparison to graphite.

The effects of bound water (as real clusters or solvation shells or in the SMD model) lead to additional polarization of the O–H bonds in surface hydroxyls and bound water molecules, especially located in the first adsorption layer, that even may lead to generation of the Eigen and Zundel cations (Figs. 8 and 9). An increase in the number of bound water molecules leads to the stabilization of these cations and a certain downfield shift in the ^{1}H NMR peak at δ_H = 15–16 ppm (Fig. 8, Eigen cation).

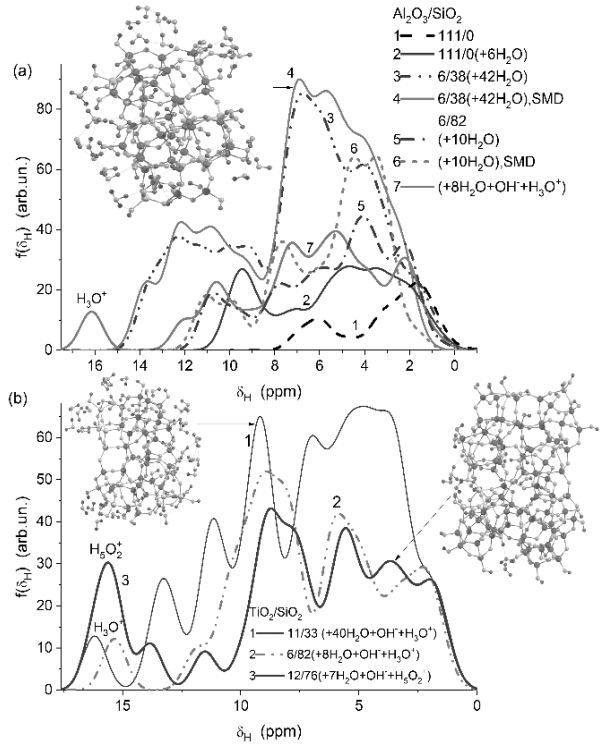

Fig. 8. ^{1}H NMR spectra of differently hydrated (*a*) γ-alumina and alumina/silica clusters and (*b*) TiO_2/SiO_2 clusters; DFT method with GIAO/ωB97X–D/cc–pVDZ (with or without solvation effects with SMD)

A position of a peak related to the Eigen cation is practically similar for Al_2O_3/SiO_2 and TiO_2/SiO_2 at X/Si = 6/82 and 12/76 with bound $10H_2O$ (Fig. 8), however, the δ_H value is slightly greater (16.1 ppm) for the Eigen cation bound to Al_2O_3/SiO_2 (Fig. 8 *a*, curve 7) than δ_H = 15.4 ppm for TiO_2/SiO_2 (Fig. 8 b, curve 2). Appearing of water bound to γ-Al_2O_3 nanoparticle results in a significant downfield shift of the ^{1}H NMR lines of the OH groups (Fig. 8 *a*, curves 1 and 2). However, the acidity of surface sites and polarized hydroxyls is greater for alumina/silica, AS (Figs. 8 and 9) than for pure alumina (Fig. 8 *a*, curves 1 and 2). Greater values of δ_H are observed for bound water (molecules directly interacting with surface sites, Fig. 9, curves 3 and 4) than that for surface hydroxyls (curves 5 and 6). The use of the SMD method (with water as a solvent) results in insignificant changes in the ^{1}H NMR spectra of bound water and surface hydroxyls (Figs. 8 and 9). These changes are greater at a smaller number of water molecules bound to oxide nanoparticles since a relative number of the H atoms with the hydrogen bonds is smaller than at a larger number of bound water molecules.

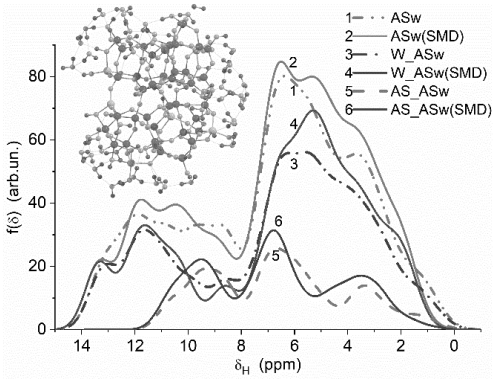

Fig. 9. ^{1}H NMR spectra of alumina/silica (11/33, 35OH) cluster with bound $42H_2O$ (curves 1 and 2), only bound water (curves 3 and 4), and surface OH groups (curves 5 and 6) (DFT method with GIAO/ωB97X–D/cc–pVDZ, with (curves 2, 4, and 6) or without (1, 3, and 5) solvation effects with SMD)

CONCLUSION

The use of the charge (CDF) and chemical shift (SDF) distribution functions for various complex nanomaterials provides a deeper insight into their electronic structure features depending on the composition of the materials, doping of a host phase by a guest phase at various amounts of dopants, structure of O– and OH–containing surface sites and other surface functionalities, amounts and organization of adsorbed water molecules, formation of charged surface sites and solvated ions (*e.g.*, H_3O^+, $H_5O_2^-$, OH^-), *etc*. The CDF of metal and hydrogen atoms (as electron-donors) are more sensitive to the mentioned factors than the CDF of O, N, and C atoms (as

electron acceptors). The use of the CDF and SDF in parallel expands the developed tool possibility in detailed analyses of the structural and interfacial effects in hydrated functionalized complex nanomaterials that is of importance on practical applications of nanostructured adsorbents, catalysts, and fillers.

ACKNOWLEDGEMENT

The author is grateful to the National Research Foundation of Ukraine ("Support of advanced and young scientists", grant 2020.02/0057) for financial support of the study.

Квантовохімічно розраховані інтегральні характеристики складних наноматеріалів

В.М. Гунько

Інститут хімії поверхні ім. О.О. Чуйка Національної академії наук України
вул. Генерала Наумова, 17, Київ, 03164, Україна, vlad_gunko@ukr.net

Розробка додаткових інструментів для аналізу електронної структури складних наноматеріалів залежно від особливостей їхньої просторової та хімічної будови являє інтерес як з практичної, так і з теоретичної точок зору. Тому в цій роботі розробляється підхід, заснований на обчисленнях функцій розподілу заряду (CDF) паралельно з розрахунками функцій розподілу хімічних зсувів (SDF) протонів, який застосовується до низки складних наноматеріалів. Бінарні нанооксиди (оксид алюмінію/діоксид кремнію, діоксид титану/діоксид кремнію та ін.), допований 3d-металами анатаз, функціоналізоване активоване вугілля, вуглецеві нанотрубки, фулерен C_{60}, оксид графену та N-легований графен розглянуто як представників різних класів комплексних наноматеріалів. Застосування CDF та SDF аналізу для складних систем дає глибші уявлення про особливості електронної будови залежно від складу матеріалів, легування головної фази допантами при різних кількостях легуючих речовин, структури O- та OH-вмісної поверхні, кількості та організації адсорбованих молекул води, утворення заряджених поверхневих функціональних груп та сольватованих іонів. CDF атомів металу та водню (донори електронів) більш чутливі до згаданих факторів, ніж CDF атомів O, N та C (акцептори електронів). Паралельне використання CDF та SDF розширює можливості детального аналізу структурних та міжфазних ефектів у гідратованих складних матеріалах.

***Ключові слова**: комплексні наноматеріали, атомні заряди, хімічний зсув протонів, функції розподілу, ТФГ методи, напівемпіричні квантовохімічні методи*

REFERENCES

1. Iler R.K. *The Chemistry of Silica*. (Chichester: Wiley, 1979).
2. Legrand A.P. (Ed.) *The Surface Properties of Silicas*. (New York: Wiley, 1998).
3. Bergna H.E., Roberts W.O. (Eds.) *Colloidal Silica: Fundamentals and Applications*. (Boca Raton: CRC Press, 2006).
4. Adamson A.W., Gast A.P. *Physical Chemistry of Surface*. 6th edition. (New York: Wiley, 1997).
5. Tapia O., Bertrán J. (Eds.) *Solvent Effects and Chemical Reactivity*. (New York: Kluwer Academic Publishers, 2000).
6. Somasundaran P. (Ed.) *Encyclopedia of Surface and Colloid Science*. Third Edition. (Boca Raton: CRC Press, 2015).
7. Henderson M.A. Interaction of water with solid surfaces: fundamental aspects revisited. *Surf. Sci. Rep*. 2002. **46**(1–8): 1.
8. Birdi K.S. (Ed.) *Handbook of Surface and Colloid Chemistry*. Third edition. (Boca Raton: CRC Press, 2009).
9. Al-Abadleh H.A., Grassian V.H. Oxide surfaces as environmental interfaces. *Surf. Sci. Rep*. 2003. **52**(3–4): 63.
10. Gun'ko V.M., Turov V.V. *Nuclear Magnetic Resonance Studies of Interfacial Phenomena*. (Boca Raton: CRC Press, 2013).

11. Gun'ko V.M., Turov V.V., Zarko V.I., Goncharuk O.V., Pakhlov E.M., Skubiszewska-Zięba J., Blitz J.P. Interfacial phenomena at a surface of individual and complex fumed nanooxides. *Adv. Colloid Interface Sci*. 2016. **235**: 108.
12. Gun'ko V.M., Turov V.V., Zarko V.I., Goncharuk O.V., Pakhlov E.M., Matkovsky O.K. Interfacial phenomena at a surface of individual and complex fumed nanooxides. *Surface*. 2019. **11(26)**: 3.
13. Guo Z., Liu B., Zhang Q., Deng W., Wang Y., Yang Y. Recent advances in heterogeneous selective oxidation catalysis for sustainable chemistry. *Chem. Soc. Rev*. 2014. **43**: 3480.
14. Canuto S. (Ed.) *Solvation Effects on Molecules and Biomolecules. Computational Methods and Applications*. (Dordrecht: Springer, 2008).
15. Advani S.G. *Processing and Properties of Nanocomposites*. (Singapore: Word Scientific Publising, 2007).
16. Stojanovic B.D. (Ed.), *Magnetic, Ferroelectric, and Multiferroic Metal Oxides*. (Amsterdam: Elsevier, 2018).
17. Pandikumar A., Rameshkumar P. (Eds.) *Graphene-Based Electrochemical Sensors for Biomolecules*. (Amsterdam: Elsevier, 2019).
18. Schleyer P.v.R. (Ed.) *Encyclopedia of Computational Chemistry*. (New York: John Wiley & Sons, 1998).
19. Dykstra C.E., Frenking G., Kim K.S., Scuseria G.E. (Eds.) *Theory and Applications of Computational Chemistry, the First Forty Years*. (Amsterdam: Elsevier, 2005).
20. Cramer C.J. *Essentials of computational chemistry: theories and models*. Second edn. (Chichester, UK: John Wiley & Sons, Ltd, 2008).
21. Helgaker T., Jorgensen P., Olsen J. *Molecular Electronic Structure Theory*. (New York: John Wiley & Sons, 2014).
22. Martin R.M., Reining L., Ceperley D.M. *Interacting Electrons: Theory and Computational Approaches*. (Cambridge, UK: Cambridge University Press, 2016).
23. Engel E., Dreizler R.M. *Density Functional Theory: An Advanced Course*. (Berlin: Springer, 2013).
24. Yang K., Zheng J., Zhao Y., Truhlar D.G. Tests of the RPBE, revPBE, τ-HCTHhyb, ωB97X-D, and MOHLYP density functional approximations and 29 others against representative databases for diverse bond energies and barrier heights in catalysis. *J. Chem. Phys*. 2010. **132**(16): 164117.
25. Becke A.D. Perspective: Fifty years of density-functional theory in chemical physics. *J. Chem. Phys.* 2014. **140**(18): 18A301.
26. Marenich A.V., Cramer C.J., Truhlar D.G. Universal solvation model based on solute electron density and on a continuum model of the solvent defined by the bulk dielectric constant and atomic surface tensions. *J. Phys. Chem. B.* 2009. **113**(18): 6378.
27. Frisch M.J., Trucks G.W., Schlegel H.B., Scuseria G.E., Robb M.A., Cheeseman J.R., Scalmani G., Barone V., Mennucci B., Petersson G.A., Nakatsuji H., Caricato M., Li X., Hratchian H.P., Izmaylov A.F., Bloino J., Zheng G., Sonnenberg J.L., Hada M., Ehara M., Toyota K., Fukuda R., Hasegawa J., Ishida M., Nakajima T., Honda Y., Kitao O., Nakai H., Vreven T., Montgomery J.A., Peralta J.E., Ogliaro F., Bearpark M., Heyd J.J., Brothers E., Kudin K.N., Staroverov V.N., Kobayashi R., Normand J., Raghavachari K., Rendell A., Burant J.C., Iyengar S.S., Tomasi J., Cossi M., Rega N., Millam J.M., Klene M., Knox J.E., Cross J.B., Bakken V., Adamo C., Jaramillo J., Gomperts R., Stratmann R.E., Yazyev O., Austin A.J., Cammi R., Pomelli C., Ochterski J.W., Martin R.L., Morokuma K., Zakrzewski V.G., Voth G.A., Salvador P., Dannenberg J.J., Dapprich S., Daniels A.D., Farkas Ö., Foresman J.B., Ortiz J.V., Cioslowski J., Fox D.J. *Gaussian 09, Revision D.01.* (Wallingford CT:Gaussian, Inc., 2013).
28. Barca G.M.J., Bertoni C., Carrington L., Datta D., De Silva N., Deustua J.E., Fedorov D.G., Gour J.R., Gunina A.O., Guidez E., Harville T., Irle S., Ivanic J., Kowalski K., Leang S.S., Li H., Li W., Lutz J.J., Magoulas I., Mato J., Mironov V., Nakata H., Pham B.Q., Piecuch P., Poole D., Pruitt S.R., Rendell A.P., Roskop L.B., Ruedenberg K. Recent developments in the general atomic and molecular electronic structure system. *J. Chem. Phys.* 2020. **152**(15): 154102.
29. Stewart J.J.P. *MOPAC2016*. Stewart Computational Chemistry. web: HTTP://OpenMOPAC.net. February 21, 2021.
30. Stewart J.J.P. Optimization of parameters for semiempirical methods VI: more modifications to the NDDO approximations and re-optimization of parameters. *J. Mol. Mod*. 2013. **19**(1): 1.
31. Gun'ko V.M. Modeling of interfacial behavior of water and organics. *J. Theor. Comput. Chem.* 2013. **12**(07): 1350059.
32. Gun'ko V.M. Interfacial phenomena: effects of confined space and structure of adsorbents on the behavior of polar and nonpolar adsorbates at low temperatures. *Current Physical Chemistry.* 2015. **5**(2): 137.
33. Gun'ko V.M. Effects of methods and basis sets on calculation results using various solvation models. *Him. Fiz. Tehnol. Poverhni.* 2018. **9**(1): 3.
34. Gun'ko V.M. Charge distribution functions for characterization of complex systems. *Him. Fiz. Tehnol. Poverhni.* 2021. **12**(1): 3.

35. Gun'ko V.M., Turov V.V. Structure of hydrogen bonds and ^{1}H NMR spectra of water at the interface of oxides. *Langmuir*. 1999. **15**(19): 6405.
36. Pawlak R., Liu X., Ninova S., D'astolfo P., Drechsel C., Liu J.-C, Häner R., Decurtins S., Aschauer U., Liu S.-X., Meyer E. On-surface synthesis of nitrogen-doped Kagome graphene. *Angew. Chem. Int. Ed.* 2021. **60**(15): 8370.
37. Gun'ko V.M. Electronic structure of anatase doped by metals calculated using translational boundary conditions and cluster approach. *Him. Fiz. Tehnol. Poverhni.* 2014. **5**(2): 119.
38. Linsebigler A.L., Lu G., Yates J.T. Photocatalysis on TiO_2 surfaces: Principles, mechanisms, and selected results. *Chem. Rev.* 1995. **95**(3): 735.
39. Fujishima A., Hashimoto K., Watanabe T. *TiO_2 Photocatalysis Fundaments and Applications*. (Tokyo: University of Tokyo, BKC, Inc., 1999).
40. Emori M., Sugita M., Ozawa K., Sakama H. Electronic structure of epitaxial anatase TiO_2 films: Angle-resolved photoelectron spectroscopy study. *Phys. Rev. B.* 2012. **85**: 035129.
41. Umebayashi T., Yamaki T., Itoh H., Asai K. Analysis of electronic structures of 3d transition metal-doped TiO_2 based on band calculations. *J. Phys. Chem. Solid*. 2002. **63**(10): 1909.
42. Wang Y., Doren D.J. Electronic structures of V-doped anatase TiO_2. *Solid State Communications*. 2005. **136**(3): 142.
43. Wu H.-C., Li S.-H., Lin S.-W. Effect of Fe concentration on Fe-doped anatase TiO_2 from GGA + U calculations. *Int. J. Photoenergy*. 2012. **2012**: 823498.
44. Du Y., Wang Z., Chen H., Wang H.-Y., Liu G., Weng Y. Effect of trap states on photocatalytic properties of boron-doped anatase TiO_2 microspheres studied by time-resolved infrared spectroscopy. *Phys. Chem. Chem. Phys*. 2019. **21**(8): 4349.
45. Gun'koV.M. Atomic charge distribution functions as a tool to analyze electronic structure of molecular and cluster systems. *Int. J. Quantum Chem*. 2021. **121**(14): e26665.

Received 25.05.2021, accepted 01.09.2021